Organic Geochemistry 41 (2010) 1235–1247

Contents lists available at ScienceDirect

Organic Geochemistry

journal homepage: www.elsevier.com/locate/orggeochem

Artificial maturation of a Type I kerogen in closed system: Mass balance and kinetic modelling

Françoise Behar [a,*], Stephanie Roy [b], Daniel Jarvie [a,c,1]

[a] Geochemistry Department, IFP Energies Nouvelles, 1-4 Avenue de Bois Préau, 92852 Rueil-Malmaison, France
[b] Petrolia, 1305 Boulevard Lebourgneuf, Québec, Canada G2K 2E4
[c] Energy Institute at TCU, PO Box 789, Humble, TX 77347, USA

ARTICLE INFO

Article history:
Received 10 February 2010
Received in revised form 23 July 2010
Accepted 18 August 2010
Available online 07 September 2010

ABSTRACT

The aim of this work was to apply a kinetic scheme proposed by Behar et al. [2008, Organic Geochemistry 39, 1–22] to a Type I kerogen of lacustrine origin. There it was demonstrated, based on experiments performed in closed pyrolysis system on a kerogen of marine source (Type II) and lignite (Type III), that the major proportion of generated hydrocarbons (Hcs) does not originate from the initial kerogen. Indeed, kerogen decomposes mainly into heavy NSO compounds. Subsequently, these NSOs rapidly undergo secondary cracking to generate hydrocarbons and a new NSO fraction. Consequently, HCs have multiple sources: a minor part comes from the kerogen itself, whereas the major part is derived from secondary cracking of the two types of NSOs. In the present work, an immature Type I kerogen was pyrolysed in a closed pyrolysis system from 275 to 350 °C with residence time between 1 h and 27 days. The kinetic scheme was optimised on the basis of the same framework as that proposed in our previous study and an excellent fit was obtained between experimental and optimised data. This kinetic scheme was used to compare our results with those obtained in open system pyrolysis and on an aliquot of the same sample matured in a closed pyrolysis system under hydrous conditions [Ruble et al., 2001, American Association of Petroleum Geologists Bulletin 85, 1333–1371]. In hydrous experiments, the results demonstrate very good prediction of the total HC fraction, which is recovered in both the tarry bitumen and the expelled oil. This means that, as far as the generation process is concerned, the rate and total amount of generated HCs are similar in both hydrous and non-hydrous closed systems. In an open system, the total HC yield is similar to that obtained in a closed system but the generation rate is significantly lower.

1. Introduction

Kerogen is formed during sediment diagenesis and is progressively thermally cracked to petroleum fluids during sediment burial. Kerogen degradation rates, amount and chemical composition of the generated products are determined under laboratory conditions by performing experiments generally above 300 °C with short residence time (less than one year). By assuming a first order kinetic law to calculate the rate constants and using the Arrhenius equation, it is possible to extrapolate laboratory results to geological conditions in which oil generation requires exposure to temperatures lower than 150 °C for millions of years.

Three types of pyrolysis systems are generally used for these experiments: open system, anhydrous closed system and hydrous closed system (Tissot and Espitalié, 1975; Monthioux et al., 1985; Serio et al., 1987; Ungerer and Pelet, 1987; Horsfield et al., 1989; Burnham and Braun, 1990; Braun and Burnham, 1990; Ungerer, 1990; Lewan, 1993, 1997; Tegelaar and Noble, 1994; Michels and Landais, 1994; Tang and Stauffer, 1994; Behar and Hatcher, 1995; Behar et al., 1997; Dieckmann et al., 2000; Schenk and Dieckmann, 2004, among others). In the three systems, it was observed that the pyrolysis products from kerogen or lignite degradation are dominated by heteroatomic compounds, called 'NSOs', of very high molecular weight (Tissot et al., 1971; Ishiwatari et al., 1977; Tissot and Welte, 1984; Teerman and Hwang, 1991; Lewan, 1993; Behar et al., 1997, 2003; Lewan and Ruble, 2002).

Behar et al. (2008a) proposed an integrated compositional kinetic schema for describing primary cracking of kerogen and secondary cracking of generated products. Artificial maturation was performed in a closed system under non-hydrous conditions. Pyrolysis products were extracted using two successive solvents: first with *n*-pentane in order to recover an extract containing saturates, aromatics and a fraction of the resins, but free of asphaltenes; then, a second extraction with dichloromethane (DCM) to recover a second fraction containing both resins and asphaltenes. The analytical distinction between these two types of NSOs is that the heavier NSOs, i.e. those only soluble in DCM, are more unstable than those soluble in *n*-pentane. This new kinetic scheme demonstrated that

* Corresponding author. Tel.: +33 1 4752 6166; fax: +33 1 4752 7019.
E-mail address: francoise.behar@ifpenergiesnouvelles.fr (F. Behar).
[1] Present address: IFP Energies Nouvelles.

0146-6380/$ - see front matter © 2010 Elsevier Ltd. All rights reserved.
doi:10.1016/j.orggeochem.2010.08.005

only a small proportion of hydrocarbons HCs are generated from kerogen itself; most are derived from cracking of generated NSOs. These results confirm previous models from Fitzgerald and van Krevelen (1959) for coal and Tissot (1969) and Ishiwatari et al. (1977) for kerogen, in which the NSOs (termed 'mesophase' by Fitzgerald and van Krevelen, 1959) are primary products of kerogen decomposition and that HCs are, in fact, generated from secondary cracking of NSOs. This kinetic scheme was also proposed by Lewan (1997), in which kerogen first decomposes into a tarry bitumen enriched in polar compounds. Then, this bitumen undergoes secondary cracking and generates the main part of HCs.

The objective of the present work was to apply this successive kinetic scheme to a typical kerogen from a lacustrine source (Type I). Thus, by adding this sample, it should be possible to determine if the same model for primary cracking can be applied to the three main types of organic matter as defined by Tissot et al. (1974).

2. Sample selection

A Type I kerogen from the Green River Formation, Uinta Basin, USA was selected. The sample is an aliquot of an immature Mahogany Shale (sample 930923-8; Ruble et al., 2001) that forms part of the Parachute Creek Member of the formation. It is thermally immature as indicated by both the Rock–Eval parameters and elemental analysis (Table 1). Prior to pyrolysis, the kerogen was isolated by dissolution of minerals in the rock with non-oxidizing acids under a nitrogen atmosphere (Durand and Nicaise, 1980). Any extractable organic matter (EOM) was removed from the kerogen by two successive extractions with DCM. The extracted kerogen was dried and stored in a glove box under a nitrogen atmosphere. Bulk pyrolysis data were acquired for the isolated kerogen using multiple heating rates with a Rock–Eval 6 instrument (Behar et al., 2001) and the resulting data files utilized to compute bulk kinetic parameters using the GeoKin software. The results show a typical mono energetic profile. The mean value of the activation energy at 56 kcal/mol (Table 2) is higher than that generally found at 54 kcal/mol (Ungerer and Pelet, 1987; Braun et al., 1992; Sundararaman et al., 1992) and corresponds to the optimised A value at $5.64 \times 10^{14}\ s^{-1}$ during error function minimisation. However, a slightly higher error function was observed for a frequency factor at $1.00 \times 10^{13}\ s^{-1}$ corresponding to an average E at 54 kcal/mol.

3. Experimental simulation in a closed pyrolysis system

3.1. Reactor description

Gold tube reactors (6 cm × 1 cm) were used to perform experiments on 250 mg aliquots of kerogen. For kerogen conversion below 5%, duplicate or triplicate experiments were carried out. For specific experiments with DCM and *n*-pentane NSOs, a mother DCM solution was prepared with a concentrate ranging between 80 and 100 mg/ml. One milliliter of the solution was deposited on a soft gold foil, previously curved and evaporated under nitrogen in a glove box for 3 days. Successive weights were measured inside the glove box until the sample reached a constant mass. The foil was then folded and transferred to a gold tube reactor.

Gold tube filling and welding were carried out under nitrogen inside a glove box. The sealed tubes were placed into an oven for isothermal heating. The pyrolysis time was initiated when the desired isothermal temperature was reached, i.e. ca. 15–20 min after placing the autoclaves in the oven. At the end of the desired reaction time, the autoclaves were cooled in a water bath and slowly depressurized so as to not rupture the gold tubes. Two tubes were used for each temperature/time condition, one for gaseous product and the other for liquid product analysis.

3.2. Mass balance

For gas analysis, gold tubes were pierced in a vacuum line equipped with a Toepler pump to isolate and measure the total quantity of gas (Behar et al., 1989). Condensable gases (CO_2, H_2S and C_2–C_4 alkanes) and permanent gases (H_2, N_2 and C_1) were recovered in a glass ampoule for a molecular characterization via gas chromatography (GC). For liquid fraction recovery, gold tube opening was carried out at room temperature under atmospheric pressure. Pyrolysis products were successively extracted first with *n*-pentane and DCM. First, the gold tube was pierced, cut into small pieces and transferred to a flask filled with *n*-pentane, which was refluxed for 1 h with constant magnetic stirring. After filtration, the *n*-pentane solution was concentrated to 10 ml and weighed for volume quantification. An aliquot of ~2 ml was weighed and used to quantify the C_6–C_{14} compounds using GC. The C_5 compounds that co-eluted with the solvent were not quantified. A second aliquot of 3 ml was evaporated and weighed before fractionation by way of liquid chromatography into saturates (Sat), aromatics (Aro) and *n*-pentane NSOs, which corresponded to resin compounds because asphaltenes are not soluble in *n*-pentane. After *n*-pentane extraction, the insoluble fraction left on the filter was extracted with DCM. This extract was verified to contained <1 wt.% of saturates and aromatics; therefore, >98% were polar compounds, which included the total asphaltene fraction and resins not soluble in *n*-pentane. After solvent evaporation, this second extract was dried and weighed. Finally, the insoluble residue, together with the gold pieces, was dried and weighed. The complete analytical procedure is summarized in Fig. 1.

The total mass balance is the following:

$$\text{Total}\ (\%) = CO_2 + H_2S + C_1{-}C_4 + C_6{-}C_{14} + C_{14+}\ \text{Sat} + C_{14+}\ \text{Aro} + n\text{-}C_5\ \text{NSOs} + \text{DCM NSOs} + \text{solid residue}.$$

In this mass balance, water generated during artificial maturation was not quantified.

3.3. Kinetic modelling

For kinetic modelling, it is assumed that thermally unstable chemical classes decompose through first order processes and rate constants depending on temperature according to the Arrhenius law. The average rate of decomposition of a chemical class can be accounted for by a set of independent, parallel reactions. Kinetic (*Ea* and *A* for each reaction in the model) and stoichiometric

Table 1
Rock–Eval data for initial Type I source rock and kerogen and elemental composition.

Whole rock							Kerogen												
TOC (%)	S1 (mg/g)	S2 (mg/g)	S3 (mg/g)	T_{max} (°C)	HI (mg/g C)	OI (mg/g C)	S2 (mg/g)	T_{max} (°C)	HI (mg/g C)	OI (mg/g C)	C (wt.%)	H (wt.%)	O (wt.%)	N (wt.%)	S (wt.%)	Fe (wt.%)	Total	Atomic ratio	
																		H/C	O/C
14.5	5.4	119.2	1.7	435	822	12	524	434	734	10	71.4	8.6	7.1	3.0	4.9	3.8	98.8	1.45	0.075

Table 2
Bulk kinetic parameters for initial kerogen using the Rock–Eval technique.

Ea (kcal/mol)	*P* (%)
48	1.1
50	0.7
52	5.7
54	12.6
56	71.8
58	4.9
60	1.8
62	0.2
64	0.5
66	0.7
Total	100.0
A (s^{-1})	5.64E+14

parameters were numerically calibrated according to pyrolysis mass balances. Optimisation was achieved with GeoKin Compositional software, an IFP kinetic simulator that allows rate parameters to be adjusted by finding the minimum of an error function, *F*, corresponding to the sum of squared differences between measured and computed amounts. The minimisation of F was performed using a modified Levenberg–Marquardt algorithm constrained by mass conservation: the sum of the stoichiometric coefficients for each reaction must equal 100%.

4. Results and discussion

4.1. Mass balance for initial kerogen

Mass balances are given in Table 3 for the total HC fraction (Total HC), which is defined as follows:

$$\text{Total HC fraction} = C_1{-}C_4 + C_6{-}C_{14} + C_{14+}\ \text{Sat} + C_{14+}\ \text{Aro}$$

Gas analysis was performed on all experiments except at 275 and 300 °C for 3 and 9 h due to the low gas yields. In each experiment, the *n*-pentane extract was successfully recovered. However, the filtration of the DCM extract was difficult and problematic in seven experiments. Thus, both the DCM extract and insoluble residue quantifications were not completed for these experiments. For the other experiments, results indicate that in most cases the total recovery was between 98% and 100%, but was lower for experiments at 350 °C. For comparison, the evaluation of the insoluble residue as determined by difference was indicated as solid residue 2.

Using bulk kinetic parameters, it was possible to determine the equivalent kerogen transformation ratio (TR) whatever pyrolysis conditions were used in the closed system. Although, this does not mean that kerogen conversion in closed system is the same as in an open system, it is a way to segregate the experimental results with increasing maturity and to determine the main successive steps of primary and secondary cracking processes in a closed system. The general trends with increasing kerogen TR for the solid residue, the n-C_5 and DCM NSOs and the total HC fraction are shown in Fig. 2.

The amount of insoluble residue (Fig. 2) shows a sharp decrease initially, reaching a minimum between 25% and 70% of kerogen transformation as defined from extrapolation of open system kinetics to these conditions. It corresponds to the thermal decomposition of the initial kerogen. Although experimental points are missing around this minimum region, it appears that a minimum of 10% insoluble residue may be reached. This indicates that almost 90% of the initial kerogen is decomposed and converted. Under the most severe conditions, the amount of insoluble residue increases, indicating that there is another source of solid residue that is being added from secondary cracking reactions. This additional source may begin adding to the residue amount before the minimum value is reached and thereby suggests that more than 90% of the initial kerogen can be thermally decomposed.

The data show that DCM NSOs are generated as soon as kerogen starts to crack, following a trend with a very steep slope for kerogen TR below 15%. In this low maturity range, the yield of the DCM NSOs reaches about 30%. However, there is insufficient experimental data to determine when the maximum yield of DCM NSOs is reached. Nonetheless, an estimation may be made. In the kerogen TR range of 35–45%, the non-HC gas yield is 3%, insoluble yield 10–0%, n-C_5 NSOs around 25% and total HC fraction around 20%. Thus, the maximum DCM NSO product is between 32% and 43%, i.e. a mean of about 37%. After this maximum, a sharp decrease in DCM NSOs is observed. These observations suggests that rapid and significant generation of the DCM NSOs occur as soon as initial kerogen begins to crack and further suggests that these compounds are likely to be primary products of kerogen decomposition, having a maximum yield higher than the estimated of 32–43%.

The *n*-pentane NSOs also are generated as soon as kerogen cracks, but the yield slope is less than that of the DCM NSOs. In our previous work, it was observed that *n*-pentane NSO compounds originated mainly from the secondary cracking of DCM NSOs. In order to verify that they are indeed not primary products, specific experiments were completed on the thermal decomposition of DCM NSOs and are described in Section 4.2.

The generation curve of the total hydrocarbon yield also starts at very early stages of kerogen cracking (TR below 3–4%) with a linear upward trend extending to a kerogen TR near 100%. The maximum HC yield is 35% of the total organic matter and is reached when kerogen conversion is complete. The relative distributions

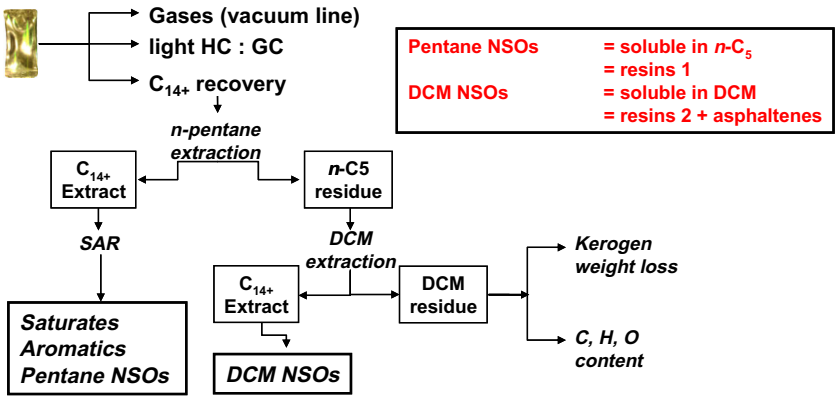

Fig. 1. Analytical procedure used in closed pyrolysis experiments for calculating total mass balance.

Table 3
Mass balance (%) for Type I kerogen matured in a closed pyrolysis system. The kerogen TR corresponds to that derived using bulk kinetics in an open system for the temperature/time conditions. Solid residue 1 is the amount recovered in the experiments, whereas solid residue 2 is calculated by difference (100-total yield). The total HC fraction = C_1–C_4 + C_6–C_{14} + C_{14+} Sat + C_{14+} Aro.

Experimental conditions		Open system	Gas fraction						HC fraction			NSOs		Solid residue 1 (by weight) (%)	Totals		Solid residue 2 (by diff.) (%)
T (°C)	t (h)	Cal. TR (%)	Non-HC		HC				C_6–C_{14} (%)	C_{14+}		DCM (%)	n-C_5 (%)		All fractions (%)	HC fractions (%)	
			CO_2 (%)	H_2S (%)	C_1 (%)	C_2 (%)	C_3 (%)	C_4 (%)		Sat (%)	Aro (%)						
275	3	0.5	–	–	–	–	–	–	–	0.2	0.3	7.8	1.2	–	–	0.5	90.5
275	9	1.3	–	–	–	–	–	–	–	0.6	0.9	10.8	3.3	82.3	97.9	1.5	84.4
275	24	2.2	1.6	0.0	0.2	0.0	0.0	0.1	–	0.9	1.4	14.3	5.3	73.1	96.9	2.6	76.2
275	72	4.0	1.7	0.0	0.2	0.1	0.1	0.1	1.1	1.2	2.0	–	6.7	–	–	4.8	–
275	216	7.9	1.9	0.0	0.3	0.1	0.1	0.1	1.5	1.7	2.7	–	9.5	–	–	6.5	–
275	648	15.3	3.3	0.1	0.1	0.2	0.2	0.3	2.7	3.0	4.3	27.3	12.2	47.1	100.8	10.8	46.3
300	3	2.2	–	–	–	–	–	–	1.0	0.9	1.3	15.6	5.4	73.7	97.9	3.2	75.8
300	9	4.1	–	–	–	–	–	–	1.2	1.1	1.9	18.7	6.8	68.5	98.2	4.2	70.3
300	24	7.7	1.8	0.0	0.3	0.1	0.1	0.1	1.5	1.6	2.5	24.1	9.4	59.7	101.2	6.2	58.5
300	72	15.2	2.2	0.1	0.2	0.2	0.2	0.2	2.1	2.9	4.4	27.8	12.0	47.9	100.2	10.2	47.7
300	216	28.6	2.7	0.2	0.1	0.4	0.4	0.3	4.5	5.3	6.9	–	21.4	–	–	17.9	–
300	648	51.5	2.8	0.3	1.1	0.8	0.8	0.5	6.2	7.4	8.7	–	23.2	–	–	25.5	–
325	3	7.2	1.7	0.1	0.3	0.1	0.1	0.1	1.0	1.5	2.5	20.4	7.3	63.6	98.7	5.6	64.9
325	9	14.6	2.0	0.1	0.4	0.2	0.1	0.1	2.4	2.9	4.6	25.7	12.5	47.8	98.8	10.7	49.0
325	24	26.1	2.7	0.0	0.7	0.2	0.2	0.2	3.7	4.4	6.1	–	19.2	–	–	15.5	–
325	72	47.9	2.8	0.2	0.9	0.6	0.5	0.4	6.5	7.2	8.4	–	23.1	–	–	24.5	–
325	216	77.0	2.8	0.3	1.4	1.0	1.0	0.6	8.6	10.2	9.0	13.4	20.8	25.9	95.0	31.8	30.9
350	1	11.6	1.9	0.1	0.4	0.1	0.1	0.1	1.5	1.9	3.1	27.3	10.4	43.5	90.4	7.2	53.1
350	3	23.0	2.3	0.1	0.6	0.3	0.3	0.2	3.0	3.6	6.0	30.1	18.1	21.7	86.3	14.0	35.4
350	9	43.2	2.7	0.2	0.7	0.3	0.5	0.4	4.8	6.1	7.8	–	23.9	–	–	20.6	–
350	24	69.0	2.7	0.2	0.9	0.6	0.7	0.6	7.1	8.4	8.8	19.7	23.3	15.2	88.2	27.1	27.0
350	72	91.8	2.8	0.2	1.4	0.9	0.9	1.2	10.8	11.5	8.7	8.2	18.4	28.5	93.5	35.4	35.0

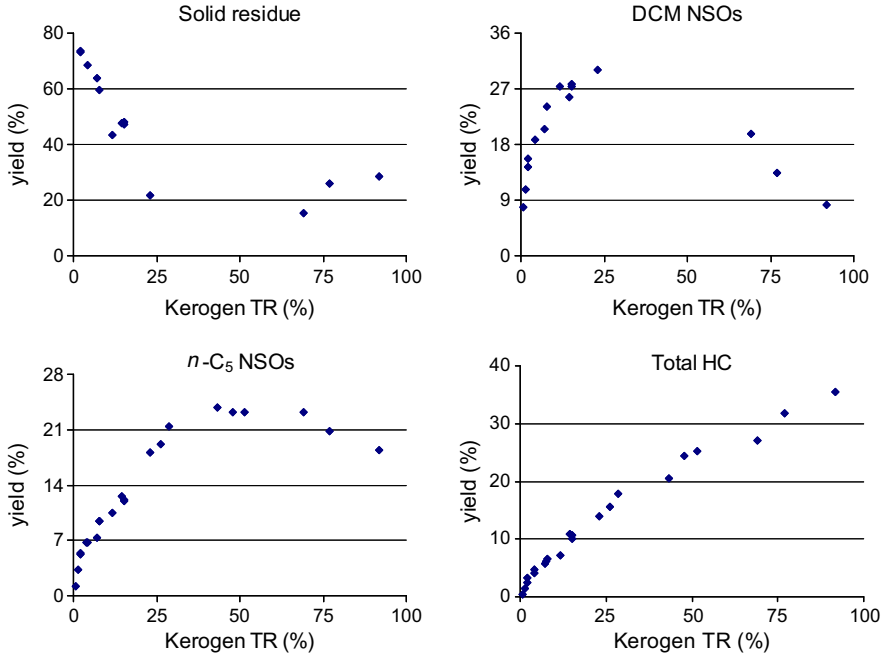

Fig. 2. Evolution of solid residue, *n*-pentane and DCM NSOs and total hydrocarbon fractions with increasing kerogen TR determined from open system kinetics.

of the hydrocarbons generated above a TR of 4% are reported in Table 4. There are no significant changes over a TR range of 4% to 23%: the C_{14+} aromatics predominate with a relative proportion of 40–44%, the light and heavy saturates in similar proportions of 19–25% and 26–29%, respectively, and hydrocarbon gases represent 7–10%. Above a kerogen TR of 30%, the relative proportion of the C_{14+} aromatics decreases continuously from 40–44% to 26%, while there is a relative increase of all other hydrocarbon classes. A maximum yield is observed for the C_{14+} aromatics whereas, for all other classes, no decrease in yield was observed. These observations suggest that, among the C_{14+} HC fraction, the aromatics are likely the most unstable class. However, a part of the C_{14+} saturates cannot be excluded from thermal cracking under these temperature/time conditions.

Table 4
Relative chemical distribution of total hydrocarbon fraction under the selected *T*/*t* conditions.

Experimental conditions		Open system	Relative hydrocarbon distribution				
			C_1–C_4 (%)	C_6–C_{14} (%)	C_{14+}		Total (%)
T (°C)	*t* (h)	Cal. TR (%)			Sat (%)	Aro (%)	
275	72	4.0	8.8	23.0	25.6	42.6	100.0
275	216	7.9	8.7	23.6	26.2	41.4	99.9
275	648	15.3	7.3	24.9	27.7	40.1	100.0
300	24	7.7	9.4	25.1	25.2	40.3	100.0
300	72	15.2	8.2	20.8	28.1	42.9	100.0
300	216	28.6	6.1	25.2	30.0	38.7	100.0
300	648	51.5	12.4	24.4	29.0	34.2	100.0
325	3	7.2	10.1	18.4	27.0	44.5	100.0
325	9	14.6	8.1	22.3	26.6	43.0	100.0
325	24	26.1	8.2	23.9	28.5	39.4	100.0
325	72	47.9	9.8	26.4	29.4	34.4	100.0
325	216	77.0	12.2	27.1	32.2	28.5	100.0
350	1	11.6	10.3	21.3	25.5	42.9	100.0
350	3	23.0	9.4	21.8	25.9	42.9	100.0
350	9	43.2	9.2	23.2	29.6	38.0	100.0
350	24	69.0	10.4	26.2	30.9	32.5	100.0
350	72	91.8	12.4	30.5	32.5	24.6	100.0

Indeed, based on kinetic parameters for saturated (Tilicheev, 1939; Ford, 1986; Dominé, 1989; Khorasheh and Gray, 1993; Song et al., 1994; Jackson et al., 1995; Behar and Vandenbroucke, 1996; Burnham et al., 1998a,b; Dominé et al., 1998) and aromatic (Savage and Klein, 1987; Freund and Olsmtead, 1989; Smith and Savage, 1991, 1994; Burnham et al., 1998a,b; Behar et al., 1999, 2002;; Yu and Eser, 1998; Lorant et al., 2000; Domke et al., 2001; Burklé-Vitzthum et al., 2003; Leininger et al., 2006, among others) model compounds or hydrocarbon mixtures (Tsuzuki et al., 1999; Behar et al., 2008b; Hill et al., 2003), it has been shown that alkylated aromatics are sensitive to thermal cracking under laboratory conditions and that C_{14+} saturates may be affected at 325 and 350 °C with times >72 h. Consequently, it is important to include these two chemical classes in the overall kinetic schema and determine the extent of their contribution to secondary cracking products under the selected *T*/*t* conditions.

In conclusion, based on the differences in thermal reactivity, two chemical types of NSOs and the total HC fractions, it is possible to propose a general kinetic scheme in which:

- The total loss of insoluble solid could reach 90% and may be more if the contribution of insoluble residue derived from DCM NSOs secondary cracking is subtracted.
- DCM NSOs are primary products from kerogen cracking and are comparatively unstable compounds.
- *n*-Pentane NSOs are generated as soon as kerogen starts to crack and it is fully necessary to determine if they are primary or secondary products.
- C_1–C_{14} hydrocarbons are stable under the selected *T*/*t* conditions, whereas the C_{14+} aromatics appear to undergo significant conversion under the most severe conditions; the thermal stability of the C_{14+} saturates needs to be checked.
- Total hydrocarbon production is observed over the entire maturity range; it can be generated from the four different sources including kerogen, DCM and *n*-pentane NSOs, and C_{14+} aromatics.

4.2. Artificial maturation of DCM NSOs

In order to better constrain the overall kinetic scheme, specific experiments were carried out on isolated DCM NSOs. For this, a large amount of the initial kerogen was pyrolysed at 275 °C for 9 h in order to generate DCM NSOs. The kerogen was then extracted with *n*-pentane followed by DCM. The recovered DCM NSOs were pyrolysed at 275, 300, 325 and 350 °C with heating times between 1 and 648 h. Mass balances are reported in Table 5. Even at the lowest temperature exposure (275 °C for 24 h or 300 °C for 9 h), 26–32% of the initial DCM NSOs were converted. This confirms the thermal instability of the DCM NSOs, as previously observed during kerogen cracking.

Table 5
Mass balances obtained for DCM NSOs generated at 275 °C/9 h and pyrolysed in closed pyrolysis system at greater severity.

Experimental conditions		Open system	Gas fraction						C_{14+} HC fraction		NSOs		Solid residue (%)	Total
			Non-HC		HC				Sat (%)	Aro (%)	DCM	*n*-C_5		
T (°C)	*t* (h)	Cal. TR (%)	CO_2 (%)	H_2S (%)	C_1 (%)	C_2 (%)	C_3 (%)	C_4 (%)						
275	24	2.2	1.2	0.1	0.1	0.1	0.1	0.0	1.6	1.4	73.7	12.2	4.1	94.6
275	72	4.0	–	–	–	–	–	–	1.8	2.2	64.4	15.7	5.9	90.0
275	648	15.3	–	–	–	–	–	–	5.4	6.2	40.1	16.9	14.7	83.3
300	9	4.1	1.0	0.1	0.2	0.1	0.1	0.1	2.3	2.6	68.0	15.5	5.3	95.3
300	24	7.7	1.4	0.2	0.3	0.2	0.2	0.2	3.2	4.1	60.0	16.7	7.8	94.3
300	216	28.6	1.9	0.2	0.7	0.5	0.5	0.4	7.4	7.7	28.5	16.0	27.7	91.5
300	648	51.5	2.2	0.4	1.0	1.0	0.9	0.8	9.7	9.0	16.9	14.0	36.2	92.1
325	9	14.6	1.7	0.2	0.5	0.3	0.3	0.3	3.4	5.6	55.6	18.8	8.8	95.5
325	648	94.1	2.3	0.4	2.2	1.8	1.6	1.5	10.3	6.5	6.6	9.8	38.0	81.0
350	1	11.6	0.9	0.1	0.3	0.2	0.1	0.1	2.5	4.7	60.2	18.4	6.4	93.9
350	24	69.0	2.2	0.4	1.5	1.2	1.1	1.3	9.0	8.5	11.3	13.1	34.2	83.8
350	216	96.8	2.4	0.4	2.9	2.3	2.1	2.2	8.6	4.8	4.8	6.3	51.2	88.0

Table 6
Bulk kinetics for DCM NSOs cracking in closed pyrolysis system.

Model A		Model B	
Ea (kcal/mol)	*P* (%)	*Ea* (kcal/mol)	*P* (%)
46	0.0	46	18.0
48	25.2	48	12.2
50	3.3	50	0.0
52	10.3	52	46.1
54	44.8	54	12.1
56	5.1	56	6.9
58	6.0	58	0.0
60	5.3	60	4.7
Total	100.0	Total	100.0
A (s^{-1})	5.64E+14	A (s^{-1}):	1.55E+14

Based on the residual amounts of recovered DCM NSOs, bulk kinetics were calculated assuming two different initial constraints: the first (Model A) imposes the same frequency factor as determined for kerogen cracking in an open system (Table 2); the second (Model B) allows the frequency factor to be optimised between 10^{10} and 10^{20} s^{-1}. The two sets of kinetic parameters are given in Table 6, with the resulting fit between measured and computed data shown in Fig. 3. The results show that the two models predict a very early thermal decomposition of the DCM NSOs, with approximately 30% cracked at activation energy below 50 kcal/mol. The main phase of thermal cracking occurs in the *Ea* range of 52–54 kcal/mol. When these values are compared with kerogen kinetics obtained in an open system, they are clearly shifted to lower values for the same frequency factor. It is worth noting that the optimised frequency factor obtained in Model B with a value of 1.55×10^{14} s^{-1} is very close to that imposed in Model A at 5.64×10^{14} s^{-1}. Moreover, the accuracy of the two models is very similar, with a correlation factor (R^2) of 0.9811 and 0.9879, respectively, due to their very similar rate constants.

In terms of pyrolysis products, the insoluble residue or prechar represents 6–8% when 30–40% of the DCM NSOs are cracked. Thus, for total conversion between 15% and 20% of prechar is expected. The yield of the *n*-pentane NSOs reaches a maximum value of 18.8% at 325 °C/9 h or 18.4% at 350 °C/1 h, which corresponds to a global DCM NSO conversion of 44% and 40%, respectively. This means that, for 100% conversion, the maximum yield will be around 45%. This value is considered as a minimum value since above 45% conversion, secondary cracking of the *n*-pentane NSOs is observed at 300, 325 and 350 °C. At conversion below 30% at 275 °C/24 h or 300 °C/9 h, the total hydrocarbon fraction represents between 4% and 5%. For a total conversion, this yield will be between 12% and 15%.

In conclusion, specific experiments carried out on isolated DCM NSOs generated from kerogen, demonstrate that they are comparatively very unstable compounds. Indeed, based on the decrease in their residual amount, bulk kinetics were derived that indicate a third of these compounds begin to decompose at activation energy as low as 46–48 kcal/mol. The optimised frequency factor at 1.55×10^{14} s^{-1} is very similar to that found at 5.64×10^{14} s^{-1} for kerogen cracking in open system pyrolysis. This validates the decision to impose this A factor value for kerogen and NSO cracking equations. In terms of stoichiometric coefficients, the following initial constrains may be proposed: between 10% and 15% for the total hydrocarbon fraction and more than 45% for the *n*-pentane NSOs and between 15% and 20% for the prechar.

4.3. Artificial maturation of n-pentane NSOs

The total *n*-pentane extract recovered from kerogen pyrolysis at 275 °C/9 h was fractionated into saturates, aromatics and NSOs. The *n*-pentane NSOs were pyrolysed at 350 °C for times between 1 and 216 h. The total mass balances are shown in Table 7. A constant decrease in the initial amount of the *n*-pentane NSOs was observed from 63.6% down to 14.5%. The rapid decrease in these compounds at 1 h indicates that there are quite unstable. By assuming the same frequency factor as for the DCM NSO decomposition, it is possible to derive an estimation of the activation energy distribution. The fit between computed and experimental conversion is shown in Fig 4. Results reported in Table 8 indicate that almost 60% of the *n*-pentane NSOs are decomposed, with activation energy between 52 and 56 kcal/mol. An equal part of 20% is much less stable, whereas 20% is more refractory.

In terms of pyrolysis product distribution, at around 50% conversion (350 °C, 3 h and 9 h), the sum of the HC gas and the C_6–C_{14} fraction is between 4% and 7%. The corresponding amount of the C_{14+} saturates is between 5% and 7%. It is interesting to note that around 15% DCM NSOs are produced, the decomposition of which lead to prechar formation. These DCM NSOs cannot be compared to those generated from the initial kerogen heated at 275 °C/9 h. Indeed, when recovered during kerogen maturation, they were mainly composed of asphaltenic compounds, whereas when generated from *n*-pentane NSO decomposition, they constitute light yellow compounds and are mainly polynuclear aromatic structures. Thus, they can be considered prechar precursors.

In conclusion, *n*-pentane NSOs are more stable than their DCM homologs. They generate at least 12% of the C_1–C_{14} and C_{14+} saturates. The sum of both prechar precursor and prechar representing around 30–0%, the amount of generated aromatics can be estimated between 30% and 40%

4.4. Elaboration of overall kinetic scheme

In order to reduce the number of free parameters and obtain an optimised kinetic scheme that was chemically consistent, the following constraints were also imposed:

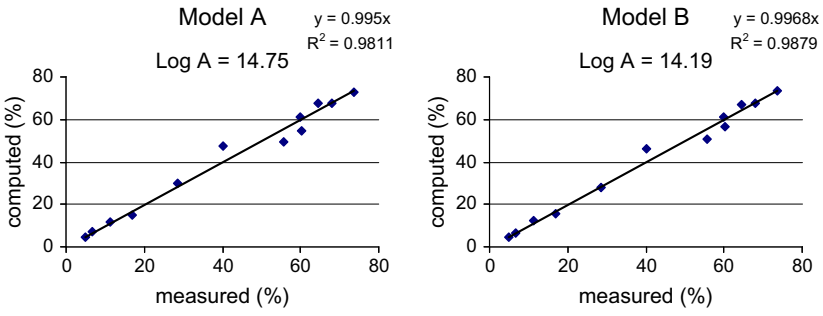

Fig. 3. Comparison between measured and computed data for global conversion of the DCM NSOs using the two sets of kinetic parameters in Table 6.

Table 7
Mass balances for *n*-pentane NSOs generated at 275 °C/9 h and pyrolysed in closed pyrolysis system at greater severity.

T (°C)	*t* (h)	Open system TR (%)	Gas fraction		C_6–C_{14}	*n*-C_5 extract			DCM	Insol. residue (%)	Total (%)	*n*-C_5 NSOs conv. (%)	Aro conv. (%)
			Non-HC (%)	HC (%)	total (%)	Sat (%)	Aro (%)	NSOs (%)	NSOs (%)				
350	1	11.6	1.3	0.6	1.4	3.3	8.4	63.6	13.6	0.0	92.3	36.4	2.3
350	2	18	1.6	1.0	1.7	3.8	8.7	55.4	15.8	0.0	88.0	44.6	4.4
350	3	23	1.8	1.4	2.3	4.6	10.1	53.1	17.3	2.9	93.4	46.9	6.5
350	9	43.2	2.3	2.8	4.0	6.6	11.9	44.1	14.1	6.4	92.2	55.9	17.4
350	24	69	2.9	4.4	4.8	8.2	10.9	30.1	14.8	7.3	83.4	69.9	36.7
350	72	91.8	2.6	5.6	6.1	9.7	10.5	21.0	8.0	19.5	83.1	79.0	67.5
350	216	96.8	3.6	7.3	7.1	7.3	6.8	14.5	5.5	35.0	86.9	85.5	94.6

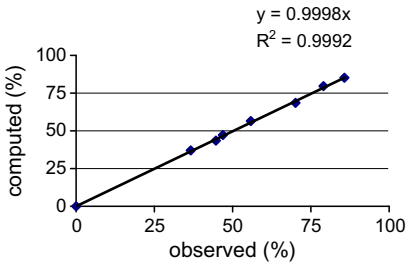

Fig. 4. Comparison between measured and computed data for *n*-pentane NSO conversion using optimised kinetic parameters in Table 8.

Table 8
Bulk kinetics for *n*-pentane NSO cracking in closed pyrolysis system.

E (kcal/mol)	*P* (%)
46	0.0
48	17.9
50	0.0
52	23.8
54	4.2
56	32.6
58	0.0
60	21.0
62	0.5
Total	100.0
A (s^{-1})	5.64×10^{14}

- Mass balances in Table 3 were split into the following nine chemical classes: non-hydrocarbon compounds (non-HC gas) including CO_2 and H_2S, stable C_1–C_{14} hydrocarbon class, C_{14+} saturates, C_{14+} aromatics, DCM NSOs, *n*-pentane NSOs, initial kerogen, residual kerogen or kerogen 2 and prechar, the solid fraction generated during the thermal cracking of the NSOs.
- The same frequency factor as determined from bulk kinetics for kerogen cracking in an open system (Table 2) was assumed for both kerogen and NSO cracking. The activation energy distribution was ascribed every 2 kcal/mol between 40 and 60 kcal/mol. Kinetic parameters for the C_{14+} aromatics and saturates thermal cracking were taken to be equal to that obtained on the same chemical classes from crude oil (Behar et al., 2008b). For the C_{14+} aromatics equation, a fourth hydrocarbon class was introduced and termed C_{14+} Aro 2, which corresponds to the new aromatics generated during their thermal cracking (Behar et al., 2008b).
- For kerogen cracking, initial estimates for stoichiometric coefficients were >80% of DCM NSOs, <10% for the kerogen 2, <5% of both *n*-pentane NSOs and hydrocarbon fractions. For DCM NSO cracking, it was anticipated that *n*-pentane NSOs are major products with a yield >50%, together with 5–15% of total HC and 20–30% of prechar.
- The relative distribution of the three hydrocarbon classes generated from kerogen and DCM NSOs was determined by averaging the distribution observed when the cracking of the C_{14+} aromatics is not yet significant, i.e. at 275 °C between 72 and 648 h and at 300 °C for 24 h and 72 h (Table 4). The resulting average composition is 30–33% for the C_1–C_{14} hydrocarbons, 26–28% for C_{14+} saturates and 39–44% for the C_{14+} aromatics.
- For the *n*-pentane NSOs decomposition, the optimised distribution of activation energy given in Table 8 was used as an initial guess. In terms of stoichiometric coefficients, the DCM NSOs, being considered prechar precursors, were lumped together with the prechar and the corresponding total yield is proposed between 30% and 40%. The same range was applied for the C_{14+} aromatics. For the C_1–C_{14} and C_{14+} saturates, values between 15% and 20% were assigned.

The optimised kinetic scheme is shown in Table 9. Results show that the initial kerogen decomposes completely to 97% DCM NSOs and 2% hydrocarbons. This means that the main result of kerogen cracking is the generation of a very viscous liquid predominated by polar compounds. As in our previous work, there is no generation of the *n*-pentane NSOs from kerogen, implying that they are secondary products. The distribution activation energy ranges from 46 to 54 kcal/mol, significantly lower than the range obtained from an open pyrolysis system of 54–56 kcal/mol. Again, the results confirm our previous results that kerogen decomposes much earlier in closed than in open system pyrolysis. As demonstrated by the experimental data, >60% of *n*-pentane NSOs are generated during the thermal cracking of the DCM NSOs with 20% prechar (solid formed from NSO and C_{14+} aromatic cracking) and 13% hydrocarbons. In terms of thermal reactivity, at least 37% of the DCM NSOs are very unstable and decompose at a very early stage of kerogen cracking. This thermal instability explains why the maximum yield of the generated DCM NSOs does not exceed 30% before decreasing, whereas the predicted yield is 97%. However, as the kinetic distribution is bimodal, a second fraction of the DCM NSOs is more stable, with activation energy between 56 and 60 kcal/mol.

The *n*-pentane NSOs generate 65% hydrocarbons and the range of the distribution energy is shifted to higher values vs. that of the DCM NSOs. The C_{14+} aromatics are slighter more unstable than those studied by Behar et al. (2008b), who proposed a partition of 21% and 79% at 52 and 54 kcal/mol. In contrast, the initial constraints for the C_{14+} saturates were not changed. In terms of relative contribution to hydrocarbon potential, 2% come from the initial kerogen, 13% from the DCM NSOs and 42% from the *n*-pentane NSOs.

The correlation between experimental and computed data for the six main classes (DCM NSOs, *n*-pentane NSOs, total HC fraction, C_1–C_{14}, C_{14+} saturates and aromatics) is shown in Fig. 5. An excellent fit is observed for all chemical classes, with almost no deviation. Indeed, the slope is very close to one, meaning that not only is the rate accurately predicted, but so the stoichiometric

Table 9
Overall kinetic schema for thermal cracking of initial kerogen together with generated unstable chemical classes and prediction of absolute yield of hydrocarbons from the different sources.

	Non-HC	HC fraction				NSOs fraction		Solid fraction		Total	Total HC	E_i (kcal/mol)	P_i (%)	A (s^{-1})
	Gas	C_1–C_{14}	C_{14}			DCM	n-C_5	Kero 2	Prechar					
			Sat	Aro 1	Aro 2									
Kerogen	0.6	0.6	0.6	0.8		97.4				100.0	2.0	46	2.0	
												48	23.2	
												52	28.9	
												54	45.9	
												Total	100.0	5.64×10^{14}
DCM NSOs	2.4	4.2	3.6	5.2			64.9		19.7	100.0	13.0	44	6.0	
												46	30.6	
												48	6.2	
												50	6.8	
												52	6.0	
												56	35.0	
												58	5.5	
												60	4.0	
												Total	100.0	5.64×10^{14}
n-C_5 NSOs	2.3	19.9	17.5	27.7					32.6	100.0	65.1	46	4.0	
												48	24.4	
												52	10.2	
												56	20.6	
												58	20.7	
												60	18.1	
												62	2.0	
												Total	100.0	5.64×10^{14}
C_{14+} Aro 1	1.3	24.3	30.0		20.4				24.0	100.0	54.3	52	25.8	
												54	74.2	
												Total	100.0	3.05×10^{13}
C_{14+} Sat		85.6			14.4					100.0	100.0	64	55.4	
												66	25.2	
												68	17.2	
												70	2.2	
												Total	100.0	3.85×10^{16}

coefficients. The fit for the two NSO classes is less accurate than for the other chemical classes. This can be explained by the experimental methodology. During the DCM extraction, the filtration procedure was not as easy as for the samples in our previous work (Behar et al., 2008a) and a part of the DCM NSOs may have been lost. During the medium pressure liquid chromatography (MPLC) fractionation of the *n*-pentane extract, a portion of the resins may be retained on the column during the back flushing procedure. For the other chemical classes, the correlation factor, R^2, is systematically between 0.98 and 0.99.

Respective conversions of the kerogen, DCM and *n*-pentane NSOs under geological conditions are shown in Fig. 6 assuming a heating rate of 2 °C/Ma. According to the kinetic scheme in Table 9, a significant part of the DCM NSOs is cracked earlier than the kerogen. Most of the *n*-pentane NSOs are more stable than both the kerogen and the DCM NSOs.

4.5. Comparison with experiments in an open system

The chemical composition of the S2 peak is given in Table 10. The pyrolysis products were quantified using the same analytical procedure as that described in Behar et al. (2008a).The calculated S2 obtained by summing the amount of both the hydrocarbons and the NSOs is larger than that directly measured by Rock–Eval 6. This can be explained by a more efficient transfer of the generated NSOs to the liquid nitrogen trap directly connected to the pyrolysis chamber. Results show that the recovered amount of NSOs (42.7%) is much lower than that predicted by the kinetic scheme for the closed system pyrolysis. On the other hand, the hydrocarbon yield at 23.3% is higher than that generated in closed system from both the kerogen and the DCM NSOs. This means that, in an open system, part of the NSOs generated from kerogen is not swept away by the carrier gas and consequently undergoes secondary cracking in the pyrolysis chamber. This observation confirmed our previous results obtained with both the Type II kerogen and Type III lignite and validated the kinetic scheme proposed for open system pyrolysis. In this kinetic scheme, the reactant is a mixture of both the initial kerogen and a part of the generated NSOs to which a complementary reaction with the same stoichiometric coefficients was added to describe the secondary cracking of the NSOs recovered in the S2 peak. This kinetic scheme was applied to the Green River Shale kerogen according to data in Table 10:

$$\text{kerogen} + (1\text{-}\alpha\ \text{NSO1}) \rightarrow 3.8\%\ \text{non-HC gas} + 23.3\ \text{HC} + 42.7\%\ \alpha\text{NSO1} + 30.2\%\ \text{kerogen 2}$$

$$42.7\ \text{NSO1} \rightarrow 1.6\%\ \text{non-HC gas} + 10.0\%\ \text{HC} + 18.2\%\ \text{NSO2} + 12.9\%\ \text{prechar}$$

The scheme can be used for simulating kerogen cracking under conditions of a closed system pyrolysis in order to compare both rate and amounts of generated HCs. As in our previous study (Behar et al., 2008a), the thermal cracking of the NSO2 was simulated

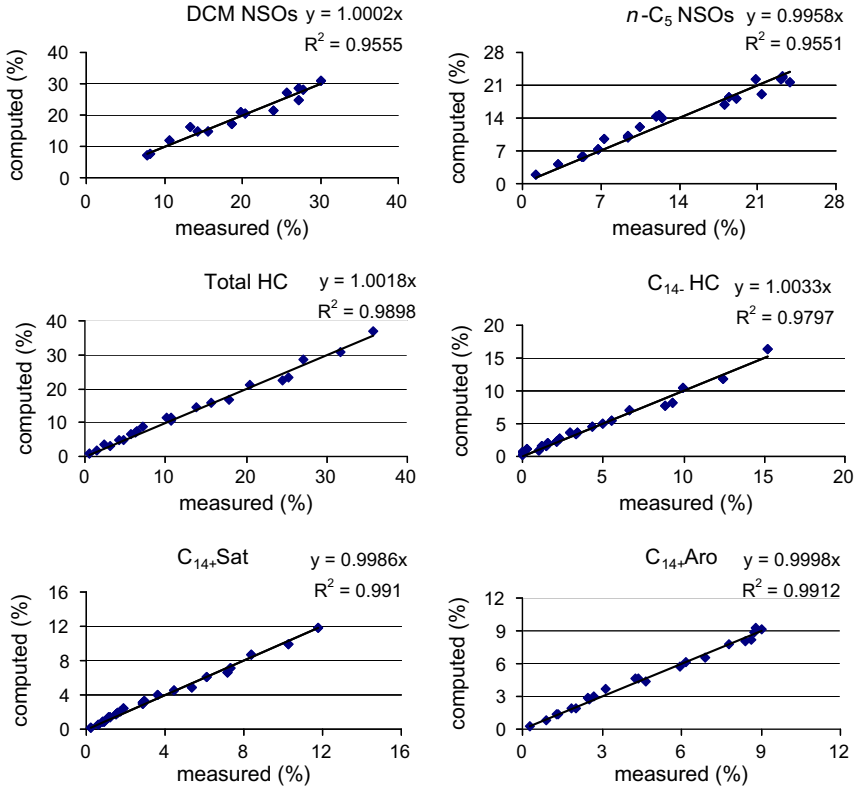

Fig. 5. Comparison between measured and computed data using overall kinetic scheme described in Table 9.

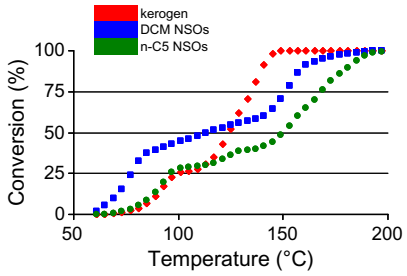

Fig. 6. Conversion of the kerogen, DCM and *n*-pentane NSOs under geological conditions (2 °C/Ma).

by considering these compounds as *n*-pentane NSOs. The different HC generations under laboratory conditions (2 °C/min) are shown in Fig. 7. Results show that the maximum HC yield is very similar in a closed system and an open system using the new kinetic scheme whereas the HC yield obtained with one reaction is significantly underestimated. Moreover, the HC rate in an open system with one or two reactions is delayed vs. to that observed in a closed system.

4.6. Comparison with hydrous experiments in a closed system

As indicated previously, the same sample selected for use in the present study was also submitted to hydrous pyrolysis in a previous study (Ruble et al., 2001). The total mass balance is given in Table 11. The amounts of each chemical class in the initial extract are higher than those obtained under less severe conditions, which exhibit constant composition at both 160 and 180 °C. Between 200 and 255 °C, the amounts of resins and asphaltenes slowly increase, indicating the very onset of kerogen cracking. Consequently, we have taken the average amounts recovered between 160 and 180 °C for the initial composition of the extract instead of those proposed by Ruble et al. (2001). Thus, the initial composition to be simulated comprises 35, 29, 51 and 13 mg/g C for the C_{14+} saturates, aromatics, resins and asphaltenes, respectively. The amount of resins was considered to be the *n*-pentane NSOs and that of asphaltenes as the DCM NSOs. For mass balance, the value obtained at 315 °C/72 h was discarded because it was out of the general trend observed for the other experiments. This initial composition was taken for predicting the experimental data using the overall kinetic scheme in Table 9. The total hydrocarbon yield estimated from the data of Ruble et al. (2001) was not easy to calculate. Indeed, in the hydrous pyrolysis workflow, the C_6–C_{14} hydrocarbons are recovered in the expelled oil, equipment and rock rinses, and tarry bitumen. The expelled oil was recovered as such and thus includes the total C_6–C_{14} hydrocarbons. During the chip drying and solvent evaporation of the equipment rinse, Ruble (1996) estimated the losses of the light fraction and added them to the total mass balances. The yield of C_6–C_{14} hydrocarbons associated with the tarry bitumen was not determined. As the specific amount of C_6–C_{14} is not given, the MPLC fractionation done on the C_{14+} fraction was applied to the total oil. This type of calcula-

Table 10
Chemical composition of S2 peak during kerogen cracking in an open system.

	Non-HC gas (%)	C_1–C_{11} (%)	C_{14+}		NSOs (%)	Total	
			Sat (%)	Aro (%)		HC (%)	S2 (mg/g)
Kerogen	3.8	11.5	6.4	5.4	42.7	23.3	659

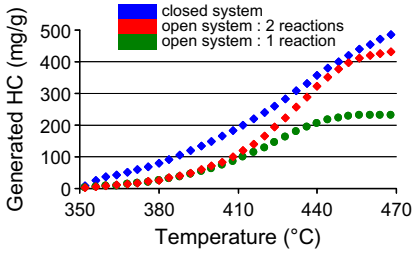

Fig. 7. comparison of HC generation under laboratory conditions (2 °C/min) in closed and open pyrolysis systems.

tion may underestimate the total hydrocarbon yield since no NSOs are present in the C_6–C_{14} fraction. The fit between the observed and computed data for the total hydrocarbon generation is given in Fig. 8a. It does not pass through the origin as the initial amount of hydrocarbons is equal to 64 mg/g C. This means that both the generation rate and the absolute yields obtained under hydrous conditions in a closed system are accurately predicted using the kinetic scheme optimised from closed system experiments under non-hydrous conditions. The correlation equation in Fig. 8a indicates that the hydrocarbon potential is slightly higher in non-hydrous conditions vs. hydrous ones. This is not surprising since the C_6–C_{14} fraction associated with the tarry bitumen was missing in the hydrous experiments and that there is not a direct estimate of the C_6–C_{14} fraction in the expelled oil. Finally, the present kinetic scheme predicts <1% kerogen conversion between 160 and 200 °C. This is in excellent agreement with experimental data in Table 11, where it is apparent that both hydrocarbons and polar compounds begin to be generated above 200 °C.

When these data are compared with those proposed by Lewan and Ruble (2002) for the hydrocarbon generation of expelled oil, there is a strong discrepancy as shown in Fig. 8b. These data include the total hydrocarbons recovered in the total mass balance and the expelled oil and tarry bitumen. Between 225 and 307.5 °C, the total generation curve matches very accurately that of the tarry bitumen. At this thermal maturity, corresponding to a kerogen conversion of 76%, the absolute hydrocarbon yield is 29 mg/g C for the expelled oil and 144 mg/g C for the tarry bitumen after subtraction of the contribution from the initial source rock extract. It is only under the most severe conditions above 345 °C that the contribution of the expelled oil becomes dominant. These observations demonstrate that in the first stage of kerogen cracking, most of the generated hydrocarbons are recovered in the tarry bitumen and then, the expelled oil. This confirms the overall kinetic scheme proposed in the present study. Indeed, it predicts that the total hydrocarbon yield for both the kerogen and the DCM NSOs is 164 mg/g C, a value very close to the maximum yield observed in Fig. 8b for the tarry bitumen, with a value at around 185 mg/g C after subtracting the initial contribution of the source rock extract. This amount represents a third of the total hydrocarbon potential and is generated much earlier than those recovered in the expelled oil. In contrast, hydrocarbon generation of the expelled oil occurs mainly when the initial kerogen has already been converted 90%. These results explain the lower rate constants proposed by Lewan and Ruble (2002). Consequently, it is not possible to take either the expelled oil or the tarry bitumen alone for comparing data with other experimental data, such as for an open system or an anhydrous system in which there is no distinction between the tarry bitumen and the expelled oil.

When this comparison is extrapolated to geological conditions (Fig. 9), the hydrocarbon generation window is larger and shifted to lower temperature using the kinetic scheme of the present study. Hydrocarbons begin to be generated around 100–125 °C and the main phase of generation occurs between 125 and 170 °C. The end of generation is observed above 175 °C, coinciding with the onset of hydrocarbon generation predicted by Lewan and Ruble (2002).

5. Conclusions

Artificial maturation of a Type I kerogen was performed under isothermal closed system pyrolysis conditions without water in the temperature range of 275–350 °C with times from 1 to 648 h. The recovery of the liquid effluents was completed by two successive extractions in order to separate the hydrocarbon fraction, NSOs soluble in *n*-pentane, and NSOs soluble in DCM. Results show that almost 90% of the initial kerogen is decomposed from thermal cracking under these condition, indicating that the insoluble resi-

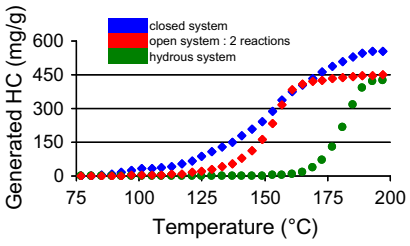

Fig. 9. Comparison of predicted hydrocarbon yield (mg/g) under geological conditions (2 °C/Ma) using the kinetic parameters proposed in Table 9 and those of Lewan and Ruble (2002).

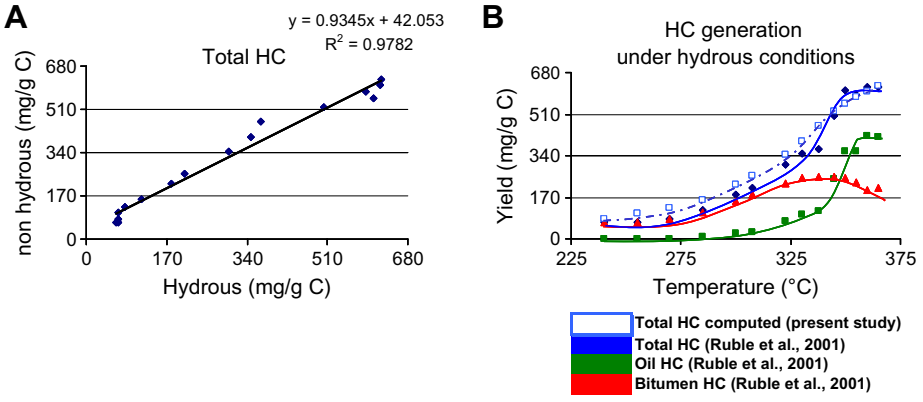

Fig. 8. (A and B) Comparison of total hydrocarbon yield predicted using the kinetic scheme proposed in Table 9 with experimental data published by Ruble et al. (2001).

Table 11
Mass balances obtained for Type I source rock artificially matured in a closed system under hydrous conditions (after Ruble et al., 2001). Kerogen conversion was determined using the kinetic scheme proposed in Table 9.

Ruble et al. (2001) Experimental conditions		Closed system Cal. TR (%)	SARA yields					HC gas yield (mg/g C)	Total hydrocarbon yield			Proportion by type	
T (°C)	t (h)		Sat (mg/g C)	Aro (mg/g C)	Res (mg/g C)	Asph	Total		Total (mg/g C)	Oil (mg/g C)	Bitumen (mg/g C)	Oil	Bitumen
Initial yields			46	32	68	35	181		78			0.00	1.00
160	72	0.0	37	29	52	14	132						
180	72	0.0	33	28	50	12	123						
Average			35	29	51	13	128						
200	72	0.4	37	33	61	15	146						
220	72	2.7	36	31	61	21	149	0	67	0	67	0.00	1.00
240	72	11.7	35	32	63	18	148	0	67	0	67	0.00	1.00
255	72	23.5	35	33	70	25	163	0	68	0	68	0.00	1.00
270	72	31.0	42	38	80	45	205	2	82	0	82	0.00	1.00
285	72	43.2	59	54	112	65	290	3	116	8	108	0.07	0.93
300	72	64.9	94	80	143	113	430	5	179	23	156	0.13	0.87
307.5	72	76.2	109	92	147	120	468	8	209	29	180	0.14	0.86
322.5	72	94.9	169	119	168	159	615	14	302	74	228	0.25	0.75
330	72	99.0	197	133	174	181	685	18	348	99	249	0.28	0.72
337.5	72	99.9	210	137	178	169	694	22	369	114	255	0.31	0.69
345	72	100.0	303	167	199	116	785	33	503	246	257	0.49	0.51
350	72	100.0	372	188	205	95	860	48	608	357	251	0.59	0.41
355	72	100.0	365	176	188	86	815	50	591	359	232	0.61	0.39
360	72	100.0	397	174	182	86	839	51	622	424	198	0.68	0.32
365	72	100.0	387	179	175	86	827	57	623	415	208	0.67	0.33

Table 12
Example of conversion for C_{14+} saturates and aromatics using the kinetic parameters indicated in Table 9.

Experimental conditions		C_{14+} HC conversion	
T (°C)	t (h)	Sat (%)	Aro (%)
275	72	0.0	0.5
275	648	0.2	4.7
300	72	0.2	4.3
300	648	2.1	28.9
325	9	0.3	3.7
325	24	0.8	9.4
325	72	2.5	24.0
325	216	7.2	49.5
350	3	0.9	7.2
350	9	2.7	19.0
350	24	7.0	39.3
350	72	18.9	69.5

due recovered under the most severe conditions originates mainly from secondary cracking reactions. The DCM NSOs are the predominant compounds generated during kerogen cracking, with a maximum yield near 30%. These compounds are very unstable, as shown from their specific pyrolysis experiments. Consequently, the products from DCM NSO thermal cracking largely overlaps that of the initial reactant, proving that the maximum yield of DCM NSOs is significantly higher than the observed one. The *n*-pentane NSOs appear to be more stable, with a maximum yield around 21%. The total hydrocarbon fraction begins to be generated at the onset of kerogen cracking and yields increase continuously with maturity. All these observations confirm the general framework of the integrated kinetic scheme we proposed in our previous work on a Type II kerogen and on a Type III lignite (Behar et al., 2008a). As such, the same sequence of successive reactions was used for elaborating the overall kinetic scheme for this Type I kerogen. The excellent fit observed between experimental and computed data for the different hydrocarbon classes and for the two types of NSOs validate this kinetic scheme. It was also shown that the C_{14+} aromatics may undergo significant secondary cracking under the T/t conditions, in contrast to the C_{14+} saturates, which only begin to be degraded under the most severe conditions. A comparison of computed conversion for these two chemical classes is shown in Table 12.

In terms of respective contributions to hydrocarbon potential, the initial kerogen generates only 2% and the total DCM NSOs adds an additional 13%. The main part originates from the thermal cracking of the *n*-pentane NSOs, which afford at 100% conversion 42%. The total hydrocarbon generation potential is 57% when the initial kerogen and the total NSO compounds are degraded.

As discussed in our previous work, this successive hydrocarbon generation during primary cracking was initially observed in oil shale retorting experiments in the early 1900s (McKee and Lyder, 1921; Franks and Goodier, 1922; Maier and Zimmerly, 1924) through the mid-1900s (Hubbaed and Robinson, 1950; Allred, 1966; Cummins and Robinson, 1972). Tissot (1969) suggested that in source rocks hydrocarbons are mainly generated from secondary cracking of NSOs. Lewan (1997) also proposed a successive kinetic scheme in which the main phase of hydrocarbon generation is due to the secondary cracking of the tarry bitumen, which is the primary product during kerogen cracking. Thus, the concept of successive steps is valid for the two types of experiments carried out in closed pyrolysis system conditions and may explain the kinetic scheme obtained for open pyrolysis system conditions. Indeed, in open system conditions, pyrolysis products are swept away from the pyrolysis chamber by the carrier gas. Thus, most of the NSOs generated from kerogen are likely to remain in the pyrolysis chamber instead of being evacuated. Consequently, the hydrocarbon generation is the result of both primary and secondary cracking reactions. In our previous work (Behar et al., 2008a), we proposed a two reaction scheme for simulating hydrocarbon generation in open system conditions. When this kinetic scheme is applied to the Green River Shale kerogen, the total HC yield is similar to that obtained in closed system conditions but the generation rate is significantly lower.

Finally, this kinetic scheme was used to simulate the experimental data obtained for hydrocarbon generation on the same Type I sample utilized by Ruble et al. (2001) but under hydrous conditions. An excellent fit was observed, meaning that water plays a minimum role on both the generation rate and the total hydrocarbon yield. Moreover, for hydrocarbon generation, those in the tarry bitumen are produced much earlier than those in the expelled oil. This difference explains why the kinetic parameters proposed by Lewan and Ruble (2002) retard hydrocarbon generation significantly over the values reported in this study.

Acknowledgement

I. Levêque is gratefully thanked for technical assistance. The authors also appreciate the helpful suggestions and comments by H. Freund and D. Curry.

Associate Editor—**C. Walters**

References

Allred, V.D., 1966. Kinetics of oil shale pyrolysis. Chemical Engineering Progress 62, 55–60.

Behar, F., Leblond, C., Saint-Paul, C., 1989. Analyse quantitative des effluents de pyrolyse en milieu ouvert et fermé. Oil and Gas Science and Technology 44, 387–411.

Behar, F., Hatcher, P.G., 1995. Artificial coalification of a fossil wood from brown coal by confined system pyrolysis. Energy and Fuels 9, 984–994.

Behar, F., Vandenbroucke, M., 1996. Experimental determination of rate constants of the n-C_{25} thermal cracking at 120, 140, and 800 bar: implication for high-pressure/high-temperature prospects. Energy and Fuels 10, 932–940.

Behar, F., Vandenbroucke, M., Tang, Y., Marquis, F., Espitalié, J., 1997. Thermal cracking of kerogen in open and closed systems: determination of kinetic parameters and stoichiometric coefficients for oil and gas generation. Organic Geochemistry 26, 321–339.

Behar, F., Budzinski, H., Vandenbroucke, M., Tang, Y., 1999. Methane generation from oil cracking: kinetics of 9-methylphenanthrene cracking and comparison with other pure compounds and oil fractions. Energy and Fuels 13, 471–481.

Behar, F., Beaumont, V., De B. Penteado, H.L., 2001. Rock-Eval 6 technology: performances and developments. Oil and Gas Science and Technology 56, 111–134.

Behar, F., Lorant, F., Budzinski, H., Desavis, E., 2002. Thermal stability of alkylaromatics in natural systems: kinetics of thermal decomposition of dodecylbenzene. Energy and Fuels 16, 831–841.

Behar, F., Lewan, M.D., Lorant, F., Vandenbroucke, M., 2003. Comparison of artificial maturation of lignite in hydrous and non-hydrous conditions. Organic Geochemistry 34, 575–600.

Behar, F., Lorant, F., Lewan, M.D., 2008a. Role of NSO compounds during primary cracking of a Type II kerogen and a Type III lignite. Organic Geochemistry 39, 1–22.

Behar, F., Lorant, F., Mazeas, L., 2008b. Elaboration of a new compositional kinetic schema for oil cracking. Organic Geochemistry 39, 764–782.

Braun, R.L., Burnham, A.K., 1990. Mathematical model of oil generation, degradation, and expulsion. Energy and Fuels 4, 132–146.

Braun, R.L., Burnham, A.K., Reynolds, J.G., 1992. Oil and gas evolution kinetics for oil shale and petroleum source rocks determined from pyrolysis-TQMS data at two heating rates. Energy and Fuels 6, 468–474.

Burklé-Vitzthum, V., Michels, R., Scacchi, G., Marquaire, P.M., 2003. Mechanistic modeling of the thermal cracking of decylbenzene. Application to the prediction of its thermal stability at geological conditions. Industrial Engineering and Chemical Research 42, 5791–5808.

Burnham, A.K., Braun, R.L., 1990. Development of a detailed model of petroleum formation, destruction, and expulsion from lacustrine and marine source rocks. Organic Geochemistry 16, 27–39.

Burnham, A.K., Gregg, H.R., Ward, R.L., Knauss, K.G., Copenhaver, S.A., Reynolds, J.G., Sanborn, R.H., 1998a. Decomposition kinetics and mechanism of n-hexadecane-1,2 $^{13}C_2$ and dodec-1-en-1,2 $^{13}C_2$ doped in petroleum and n-hexadecane. Geochimica et Cosmochimica Acta 61, 3725–3737.

Burnham, A.K., Sanborn, R.H., Gregg, H.R., 1998b. Thermal dealkylation of dodecylbenzene and dodecylcyclohexane. Organic Geochemistry 28, 755–758.

Cummins, J.J., Robinson, W.E., 1972. Thermal Degradation of Green River Kerogen at 150–350 °C – Rate of Product Formation. US Bureau of Mines Report of Investigation 7620, 15 p.

Dieckmann, V., Horsfield, B., Schenk, H.J., 2000. Heating rate dependency of petroleum-forming reactions: implications for compositional kinetic prediction. Organic Geochemistry 31, 1333–1348.

Domke, S.B., Pogue, R.F., Van Neer, F.J.R., Smith, C.M., Wojciechowski, B.W., 2001. Investigation of the kinetics of ethylbenzene pyrolysis using a temperature-scanning reactor. Engineering and Chemical Research 40, 5878–5884.

Dominé, F., 1989. Kinetics of hexane pyrolysis at very high pressure. 1. Experimental study. Energy and Fuels 3, 89–96.

Dominé, F., Dessort, D., Brevart, O., 1998. Towards a new method of geochemical kinetic modelling: implications for the stability of crude oils. Organic Geochemistry 28, 597–612.

Durand, B., Nicaise, G., 1980. Procedure of kerogen isolation. In: Durand, B. (Ed.), Kerogen, Insoluble Organic Matter from Sedimentary Rocks. Editions Technip, Paris, pp. 13–34.

Fitzgerald, D., Van Krevelen, D.W., 1959. Chemical structure and properties of coal: the kinetics of coal carbonization. Fuel 38, 17–37.

Ford, T.J., 1986. Thermal decomposition of hexadecane: reaction mechanism. Industrial Engineering and Chemical Research 25, 240–243.

Franks, A.J., Goodier, B.D., 1922. Preliminary study of the organic matter of Colorado Oil Shales. Quarterly of the Colorado School of Mines 17, 3–16.

Freund, H., Olsmtead, W.N., 1989. Detailed chemical kinetic modelling of butylbenzene pyrolysis. International Journal of Chemical Kinetics 21, 561–574.

Hill, R.J., Tang, Y., Kaplan, I.R., 2003. Insights into oil cracking based on laboratory experiments. Organic Geochemistry 34, 1651–1672.

Horsfield, B., Disko, U., Leibtner, F., 1989. The micro scale simulation of maturation: outline of a new technique and its potential application. Geologische Rundschau 78 (1), 361–374.

Hubbaed, A.B., Robinson, W.E., 1950. A thermal decomposition study of Colorado oil shale. US Bureau of Mines Report of Investigation 4744, 24 p.

Ishiwatari, R., Ishiwatari, M., Rohrback, B.G., Kaplan, I.R., 1977. Thermal alteration experiments on organic matter from recent marine sediments in relation to petroleum genesis. Geochimica Cosmochimica Acta 41, 815–828.

Jackson, K.J., Burnham, A.K., Braun, R.L., Knauss, K.G., 1995. Temperature and pressure dependence of n-hexadecane cracking. Organic Geochemistry 10, 941–953.

Khorasheh, F., Gray, M.R., 1993. High-pressure thermal cracking of n-hexadecane. Industrial Engineering and Chemical Research 32, 1853–1863.

Leininger, J.P., Lorant, F., Minot, C., Behar, F., 2006. Mechanism of 1-methylnaphthalene pyrolysis in a batch reactor and relevance with other methylated polyaromatics. Energy and Fuels 20, 2518–2530.

Lewan, M.D., 1993. Laboratory simulation of petroleum formation: hydrous pyrolysis. In: Engel, M.H., Macko, S. (Eds.), Organic Geochemistry Principles and Applications. Plenum, New York, pp. 419–442.

Lewan, M.D., 1997. Experiments on the role of water in petroleum formation. Geochimica et Cosmochimica Acta 61, 3691–3723.

Lewan, M.D., Ruble, T.E., 2002. Comparison of petroleum generation kinetics by isothermal hydrous and non-isothermal open-system pyrolysis. Organic Geochemistry 33, 1457–1475.

Lorant, F., Behar, F., Vandenbroucke, M., Mc Kinney, D.E., Tang, Y., 2000. Methane generation from methylated aromatics: kinetic study and carbon isotope modelling. Energy and Fuels 14, 1143–1155.

Maier, C.G., Zimmerly, S.R., 1924. The chemical dynamics of the transformation of the organic matter to bitumen in oil shale. University of Utah Bulletin 14, 62–81.

McKee, R.H., Lyder, E.E., 1921. The thermal decomposition of shale: I-Heat effects. The Journal of Industrial and Engineering Chemistry 13, 613–618.

Michels, R., Landais, P., 1994. Artificial coalification–comparison of confined pyrolysis and hydrous pyrolysis. Fuel 73, 1691–1696.

Monthioux, M., Landais, P., Monin, J.C., 1985. Comparison between natural and artificial maturation series of humic coal from the Mahakam Delta, Indonesia. Organic Geochemistry 8, 275–292.

Ruble, T.E., 1996. Geochemical Investigation of the Mechanisms of Hydrocarbon Generation and Accumulation in the Uinta basin, Utah. PhD. Thesis, University of Oklahoma.

Ruble, T.E., Lewan, M.D., Philp, R.P., 2001. New insights on the Green River petroleum system in the Uinta basin from hydrous pyrolysis experiments. American Association of Petroleum Geologists Bulletin 85, 1333–1371.

Savage, P.E., Klein, M.T., 1987. Asphaltene reaction pathways. 2. Pyrolysis of n-pentadecylbenzene. Industrial and Engineering Chemistry Research 26, 488–494.

Schenk, H.J., Dieckmann, V., 2004. Prediction of petroleum formation: the influence of laboratory heating rates on kinetic parameters and geological extrapolations. Marine and Petroleum Geology 21, 79–95.

Serio, M.A., Hamblen, D.G., Markham, J.R., Solomon, P.R., 1987. Kinetics of volatile product evolution in coal pyrolysis: experiment and theory. Energy and Fuels 1, 138–152.

Smith, C.M., Savage, P.E., 1991. Reactions of polycyclic alkylaromatics: structure and reactivity. American Institute of Chemical Engineers Journal 37, 1613–1624.

Smith, C.M., Savage, P.E., 1994. Reactions of polycyclic alkylaromatics. 6. Detailed chemical kinetic modelling. Chemical Engineering Science 49, 259–270.

Song, C., Lai, W., Schobert, H.H., 1994. Condensed-phase pyrolysis of the n-tetradecane at elevated pressures for long duration. Products and reaction mechanism. Industrial and Engineering Chemistry Research 33, 534–547.

Sundararaman, P., Merz, P.H., Mann, R.G., 1992. Determination of kerogen energy distribution. Energy and Fuels 6, 793–803.

Tang, Y., Stauffer, M., 1994. Multiple cold trap pyrolysis gas chromatography: a new technique for modeling hydrocarbon generation. Organic Geochemistry 22, 863–872.

Teerman, S.C., Hwang, R.J., 1991. Evaluation of the liquid hydrocarbon potential of coal by artificial maturation techniques. Organic Geochemistry 17, 749–764.

Tegelaar, E., Noble, R.A., 1994. Kinetics of hydrocarbon generation as a function of the molecular structure of kerogen as revealed by pyrolysis-gas chromatography. Organic Geochemistry 22, 543–574.

Tilicheev, M.D., 1939. Kinetics of cracking hydrocarbons under pressure. First article. Cracking of normal paraffin hydrocarbons. Foreign Petroleum Technology 7, 209–224.
Tissot, B., 1969. Premières données sur les mécanismes et la cinétique de la formation du pétrole dans les bassins sédimentaires. Simulation d'un schéma réactionnel sur ordinateur. Oil and Gas Science and Technology 24, 470–501.
Tissot, B., Califet-Debyser, Y., Deroo, G., Oudin, J.L., 1971. Origin and evolution of hydrocarbons in Early Toarcian shales. American Association of Petroleum Geologists Bulletin 55, 2177–2193.
Tissot, B., Durand, B., Espitalié, J., Combaz, A., 1974. Influence of the nature and diagenesis of organic matter in formation of petroleum. American Association of Petroleum Geologists Bulletin 58, 499–506.
Tissot, B., Espitalié, J., 1975. L'évolution de la matière organique des sédiments: application d'une simulation mathématique. Oil and Gas Science and Technology 24, 470–501.
Tissot, B., Welte, D.H., 1984. Petroleum Formation and Occurrence, 2nd ed. Springer Verlag, Berlin.
Tsuzuki, N., Takeda, N., Susuki, M., Yokoi, K., 1999. The kinetic modeling of oil cracking by hydrothermal pyrolysis experiments. International Journal of Coal Geology 39, 227–250.
Ungerer, P., Pelet, R., 1987. Extrapolation of the kinetics of oil and gas formation from laboratory experiments to sedimentary basins. Nature 327, 52–54.
Ungerer, P., 1990. State of the art of research in kinetic modelling of oil formation and destruction. Organic Geochemistry 16, 1–25.
Yu, J., Eser, S., 1998. Thermal decomposition of jet fuel compounds under-near critical and supercritical conditions. 2. Decalin and tetralin. Industrial and Engineering Chemistry Research 37, 4601–4608.